Journal of Applied Electrochemistry (2022) 53:285–295
https://doi.org/10.1007/s10800-022-01780-0

RESEARCH ARTICLE

Metal-free oleic acid-derived carbon dots as efficient catalysts for hydrogen evolution reaction

Vishal Rimal[1] · Susanta Sinha Mahapatra[1] · Prem Kumar Srivastava[1]

Received: 28 April 2022 / Accepted: 2 October 2022 / Published online: 15 October 2022

Abstract

Hydrogen evolution reaction (HER) is of high priority at present. Existing research has involved the use of noble metals as catalysts for HER, thus putting an urgency to develop low-cost materials to replace them. In this work, metal-free Oleic acid functionalized Carbon Dots have been for the first time reported to have outstanding activity for HER. Electrochemical investigation reveals excellent catalytic performance with overpotential of 1 mV at a current density of − 5 mA cm^{-2}. The performance at this range marks a significant milestone and paves the way for a sustainable future of metal-free catalysis.

Graphical abstract

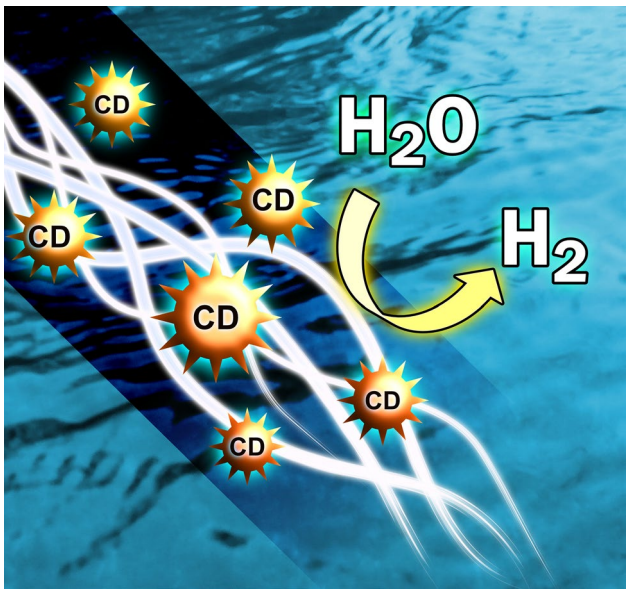

Keywords Carbon dots · Oleic acid · Metal-free · Catalyst · Hydrogen evolution reaction (HER)

1 Introduction

The strong dependence on fossil fuels and their finite availability has increasingly prompted researchers to explore green and renewable alternatives. Hydrogen is a clean and sustainable source of energy. It is the lightest fuel, has the best energy per unit mass and unlike electricity, can be easily stored [1]. Hydrogen Evolution Reaction (HER) plays a vital

✉ Susanta Sinha Mahapatra
ssmahapatra@bitmesra.ac.in

Prem Kumar Srivastava
pksrivastava@bitmesra.ac.in

[1] Department of Chemistry, Birla Institute of Technology, Mesra, Ranchi 835215, India

role in the electrocatalytic water-splitting reaction for efficient hydrogen production. The splitting of water is slow and requires a catalyst to trigger proton reduction with minimum overpotential to increase the reaction rate. Pt-based materials are considered the best choice for HER but their limited availability and high costs restrict their widespread use [2]. Transition-metal catalysts based on Fe, Co, Ni, Mo have also been explored for their catalytic activities; nevertheless, the dissociation of water in alkaline solution, which is a crucial step in HER is complex with these materials [3].

Carbon has been applied in various forms as electrocatalysts for HER, including but not limited to graphene, carbon nanotubes, carbon nanofibers, carbon spheres, carbon nanocages, etc. [4]. Carbon Dots (CDs) are nanodimensional quasi-spherical particles with a size of less than 10 nm and contain sp^2/sp^3 hybridized carbon with an array of functional groups like –COOH, –OH, $–NH_2$, etc [5]. CDs can be prepared by two approaches, namely the bottom-up and top-down. The former utilizes organic monomer/polymer precursors while the latter uses carbon materials likes graphite or carbon nanotubes (CNTs) [6]. Suitable heteroatom doping viz. N, P, S, O, etc., can be achieved to tune the properties of CDs [7]. CDs have a high surface area, excellent conductivity and rich functional groups which help form new active sites thereby boosting the dissociation of water. CDs also enhance electron transfer and improve stability thus making them excellent for catalytic applications [3, 8].

For the first time, we report that metal-free oleic acid functionalized CDs show outstanding catalytic activity for HER in alkaline conditions. The synthesis is fast, easy and highly cost-effective. Oleic acid was taken as the carbon precursor with ethylenediamine, boric acid, phosphoric acid, urea, thiourea and sulfuric acid as dopants. In order to study the influence of metal doping, $RuCl_3{\cdot}3H_2O$ was used. The use of rotating disk electrode, glassy carbon electrode and annealing process was avoided to understand the electrocatalytic behavior of CDs in a standard three-electrode system. The aforementioned reason may be the probable cause for our results to deviate from previously reported studies. The authors believe that the results presented here shall help in the development of hydrogen as an ideal fuel for a sustainable future.

2 Experimental details

2.1 Materials

Oleic acid [Qualigens Fine Chemicals], NaOH [Rankem], ethylenediamine [Merck], boric acid [Rankem], phosphoric acid [Rankem], urea [CDH], thiourea [Thomas Baker], sulfuric acid [Rankem], $H_2PtCl_6{\cdot}6H_2O$ [Sigma-Aldrich], KOH [Rankem] and $RuCl_3{\cdot}3H_2O$ of analytical grade were used as received. Double-distilled water was used in all experiments.

2.2 Methodology

2.2.1 Synthesis of oleic acid CDs

The synthesis methodology of oleic acid CDs involved the bottom-up synthesis method as reported by our group [9]. 2 g of NaOH was dissolved in 20 mL of water and stirred till a transparent solution was obtained. 10 mL of oleic acid was heated at a temperature of 260 °C for a few minutes. NaOH and oleic acid were then mixed and filtered. The aqueous dispersion of oleic acid CDs was sonicated for 15 min and subsequent functionalization and tests were performed.

2.2.2 Functionalization of oleic acid CDs

The functionalization was achieved by treating 10 mL of oleic acid CDs with 40 µL of ethylenediamine at 70 °C for 12 h in an oven. Using the same ratio and conditions boric acid, phosphoric acid, urea, thiourea, sulfuric acid were also functionalized (Fig. 1). The synthesized CDs are mentioned in abbreviated forms hereafter; (ethylenediamine: EDA-CDs,

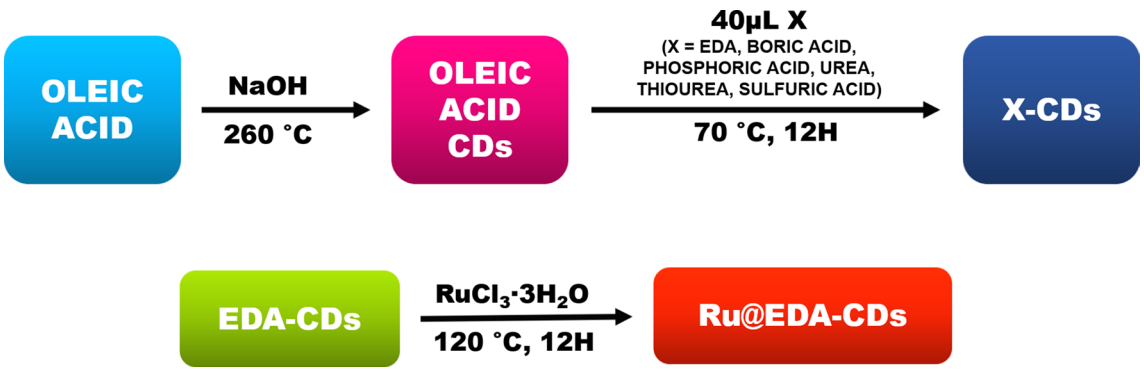

Fig. 1 Schematic showing the synthesis of CDs

boric acid: B-CDs, phosphoric acid: P-CDs, urea: U-CDs, thiourea: TU-CDs, sulfuric acid: S-CDs). The aqueous dispersion of functionalized CDs was then sonicated for 15 min and subjected to further investigation. Anhydrous CDs for electrochemical analysis was obtained by heating 4 mL of the CDs solution in an oven till evaporation.

2.2.3 Synthesis of Ru@EDA-CDs

To synthesize Ru@EDA-CDs, 7.5 mg of $RuCl_3{\cdot}3H_2O$ was mixed with 5 mL of EDA-CDs and heated in an autoclave at 120 °C for 12 h. The resulting filtrate was washed with ethanol several times and then dried at 70 °C for 12 h.

2.2.4 Preparation of Pt/C

The electrode was prepared from the precursor solution of $H_2PtCl_6{\cdot}6H_2O$ (0.1 M) by galvanostatic method at a current density of 5 mA cm^{-2} for 5 min.

2.3 Characterization

2.3.1 Instrumentation

UV–Visible absorption spectra were evaluated on LabIndia UV 3200 using a 1 cm path length quartz cuvette. PerkinElmer LS 55 was employed for fluorescence spectra. Fourier transform infrared spectrophotometer (Bruker Alpha) was used for the infrared spectrum. The morphological characterization was performed using FESEM (Zeiss). The electrochemical investigation was done with Autolab 302N.

2.3.2 Electrocatalytic activity

The electrochemical analysis was carried out in a three-electrode cell system at room temperature with a platinum rod as the counter electrode, Ag/AgCl as the reference electrode, and graphite electrode as the working electrode. 1 M KOH aqueous solution was used as the electrolyte. The coating of CDs on the working electrode was done as follows: ethanol suspensions containing 500 µL ethanol, 3 mg of catalyst, and 50 µL 5 wt % Nafion solutions were sonicated for 30 minutes. 30 µL of the resulting solution was then coated onto the graphite electrode of area 0.48 cm^2, thereby giving the electrode a loading of approximately 2.5 mg. The overpotential against Ag/AgCl was converted to reversible hydrogen electrode (RHE) using the relation:

$$E_{\mathrm{RHE}} = E_{\mathrm{Ag/AgCl}} + 0.059pH + E^0{}_{\mathrm{Ag/AgCl}}$$

where, E_{RHE} is the converted potential vs. RHE, $E^0{}_{\mathrm{Ag/AgCl}} = 0.1976$ at 25 °C, and $E_{\mathrm{Ag/AgCl}}$ is the experimentally measured potential against Ag/AgCl reference.

Table 1 Absorption and photoluminescence peaks of synthesized CDs

Sample	UV–Vis peak (nm)	PL peak (nm)
O-CDs	272	399
EDA-CDs	270	400
B-CDs	265	399
P-CDs	261	399
U-CDs	263	400
TU-CDs	–	399
S-CDs	267	403

Linear sweep voltammetry was performed with a scan rate of 5 mV s^{-1}. Cyclic voltammetry was conducted at a sweep rate of 50 mV s^{-1}. The Tafel slope were obtained from LSV curves based on the Tafel equation.

$$\eta = a + b\,log|j|$$

where, η is overpotential, a is intercept, b is Tafel slope and j is current density.

3 Results and discussion

3.1 CDs characterization

3.1.1 UV–Visible and fluorescence spectral analyses

UV–Vis analysis was performed to understand the optical properties of CDs. Figure 2 shows the UV–Vis spectra of the synthesized CDs. It is well known that the absorption spectrum of CDs generally exhibits two distinguishable peaks at around 250 and 300 nm, indicating π–π^* and n–π^* transitions respectively. The peaks corresponding to UV–Vis and PL are mentioned in Table 1. The synthesized CDs excluding TU-CDs were found to exhibit similar UV–Vis curves with a broad absorption that extended into the visible region. The absorption peaks shown by the CDs at around 270 nm is attributed to the carbonic core center [10]. Although the ratio of dopants for functionalization was constant in all cases, the absorption peak was found to be absent in the case of TU-CDs. The absence of absorption can be ascribed to the potential role of sulfur atom present in thiourea or the absence of oxygen atom since a successful synthesis was achieved using urea (U-CDs) and sulfuric acid (S-CDs) (Fig. 3). The physical and chemical similarity between urea and thiourea has been summed up in Table S1. This result puts a critical note on the influence of sulfur compounds devoid of oxygen atoms on the absorption spectra of CDs.

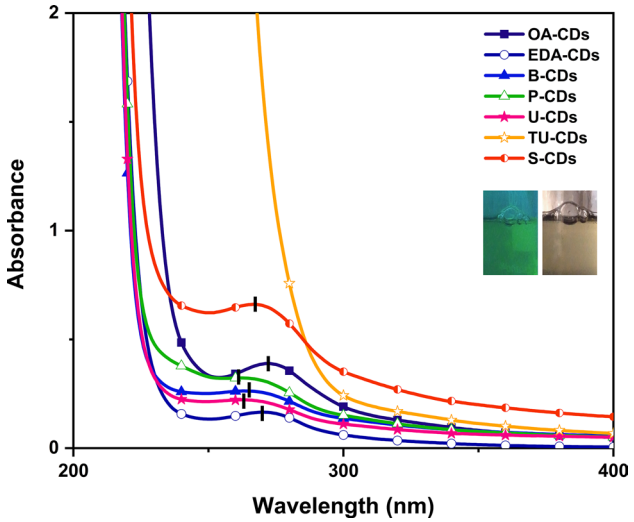

Fig. 2 UV–Vis spectra of CDs. Inset shows OA-CDs in UV and visible light

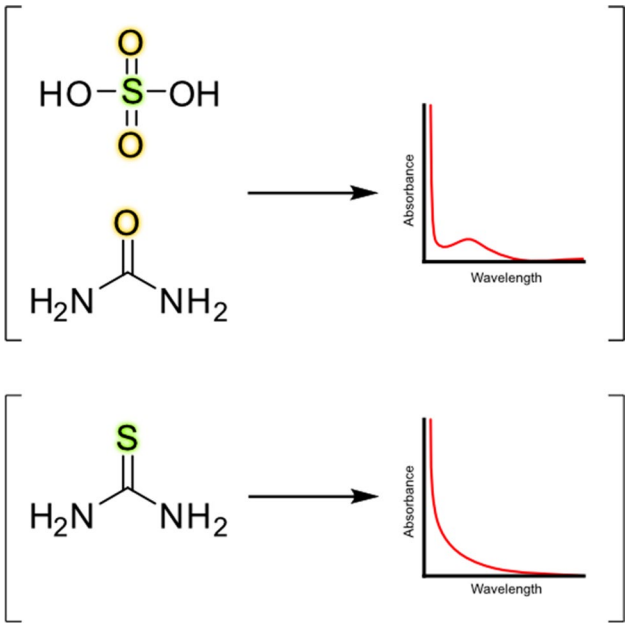

Fig. 3 Figure illustrating the possible influence of sulfur compounds devoid of oxygen on the UV–Vis spectra of CDs

CDs photoluminescence (PL) is also an important field of study because many applications rely on this property. Several manuscripts pertaining to the PL of CDs have been reported over the years; however, the origin of fluorescence remains unclear [11]. The synthesized CDs samples had maximum fluorescence intensity at approximately 400 nm at an excitation of 400 nm (Fig. 4).

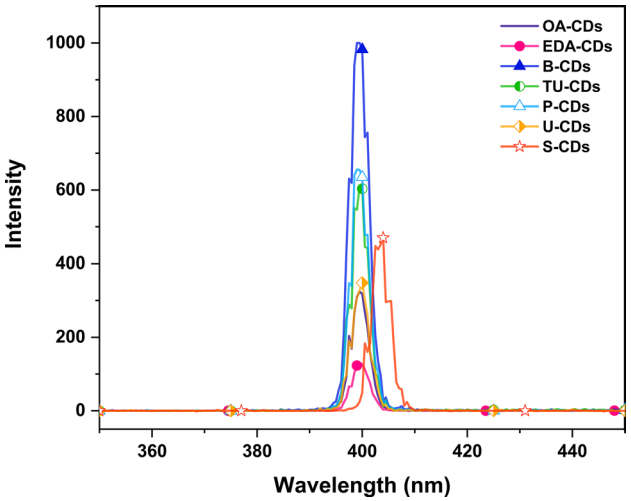

Fig. 4 Fluorescence spectra of CDs

3.1.2 FESEM analysis

The morphological investigation of CDs was done using FESEM and is presented in Fig. 5. It can be seen that doping has a considerable effect on the structural features of CDs and results in distinctive shape, with the samples showing spheroidal agglomeration and/or rod-like patterns. OA-CDs, EDA-CDs and P-CDs do not possess any tubular fragments in their structure in the tested dimensions. U-CDs and TU-CDs are seen with rod-like patterns; however, no spherical clumps can be observed. Amongst the investigated species, B-CDs and S-CDs have branched tubular structures emerging between globular clusters. Standing parallel with subsequent discussion in "Effect of CDs on graphite electrode", this unique morphological feature of B-CDs and S-CDs can be said to adequately play a potential role in increasing the surface area, thus improving the HER kinetics.

3.1.3 FT-IR analysis

FT-IR spectra (Fig. 6) of OA-CDs, B-CDs, P-CDs, S-CDs, EDA-CDs, U-CDs and TU-CDs were found to be parallel, with peaks at 3300 cm^{-1}, 2068 cm^{-1}, 1638 cm^{-1} corresponding to –OH stretching, combination bands and –OH scissoring, respectively. All the synthesized CDs excluding EDA-CDs had a prominent peak at 1389 cm^{-1} corresponding to C–O–H bending. P-CDs had an additional peak at 1002 cm^{-1}, indicating the stretching P–O vibrations [12]. Similarly, at 1094 cm^{-1} S-CDs show notable S=O stretching [13]. Comparing the distinctive peaks demonstrated

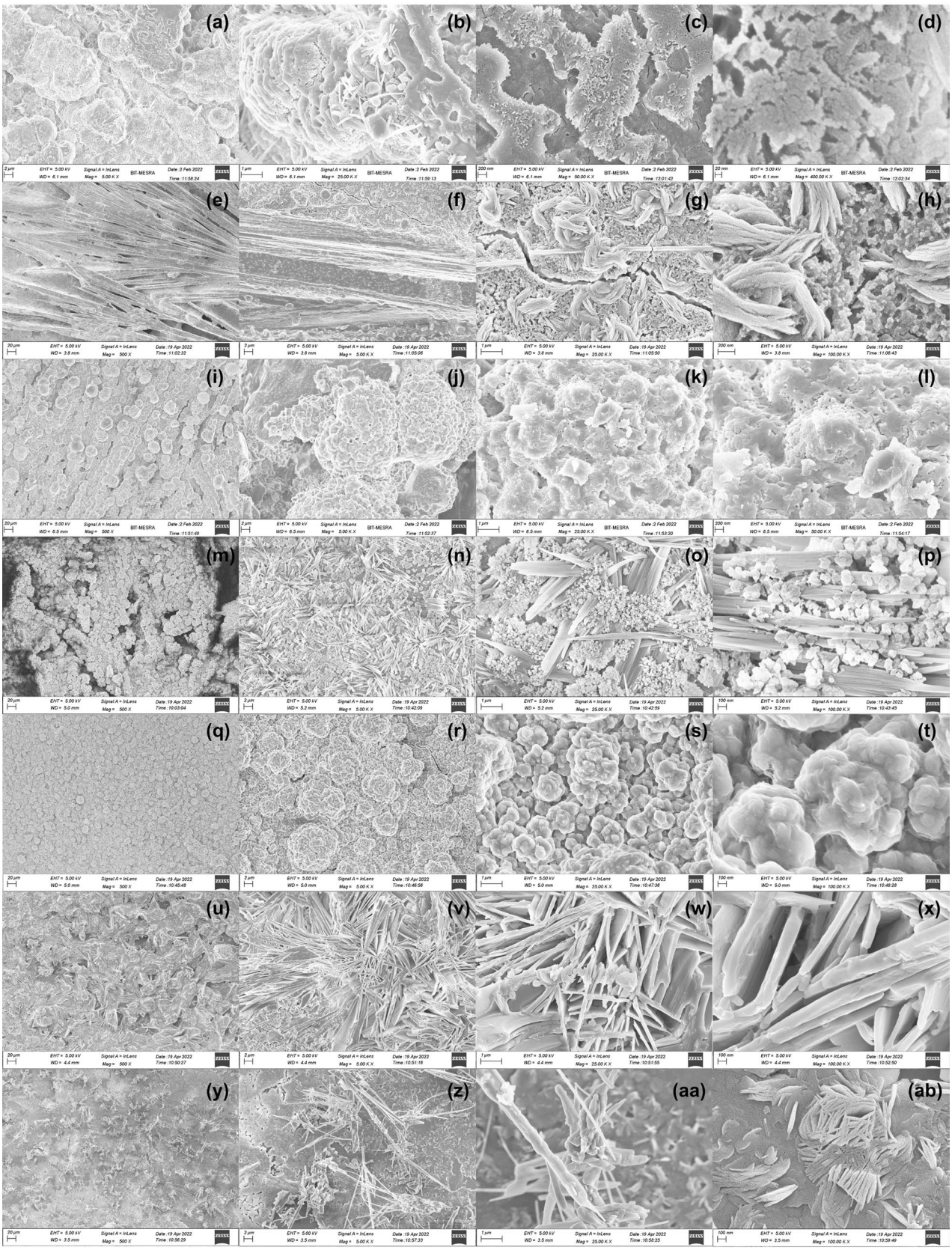

Fig. 5 FESEM images of **a–d** OA-CDs, **e–h** B-CDs, **i–l** EDA-CDs, **m–p** S-CDs, **q–t** P-CDs, **u–x** U-CDs, **y–ab** TU-CDs at different magnifications

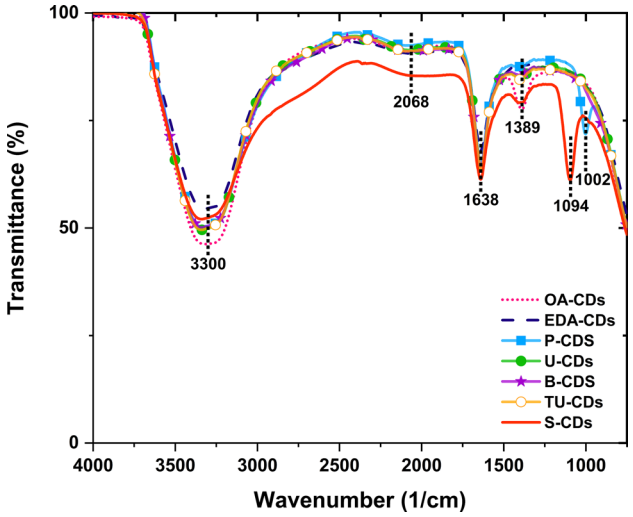

Fig. 6 FT-IR spectra of CDs

by EDA-CDs, P-CDs and S-CDs, a mechanistic inference can be observed and the same has been illustrated in Fig. 7. When carboxylic acid based CDs are reacted with species absent of –OH moieties the carboxylic –OH bond combines with the H of the reacting species, eliminating water and making way for the attachment of the dopant. In EDA-CDs the mechanism is expected to proceed via amide coupling reaction [14]. Likewise, in P-CDs, S-CDs the reacting doping species i.e., phosphoric acid and sulfuric acid have an –OH bond at disposal for reaction with OA-CDs; thus the C–O–H bending remains undisturbed in this case. The reaction most expectedly proceeds via the interaction of doping species with the independent H bonds. The same can be confirmed since additional P–O vibrations and S=O stretching are prominently recorded in the FT-IR spectra. In the absence of –OH bonds of doping species the –COOH group of CDs preferentially react however the –COOH group remains unreactive in case of the availability of –OH in the functionalizing species putting the idea that a lower energy barrier is expected for the latter thereby yielding the major product. The low transmittance of C–O–H bending in the case of P-CDs also validates that a minor fragment of doping also proceeds via the interaction with –COOH group.

3.2 Electrochemical analysis

3.2.1 Effect of CDs on graphite electrode

We measured the HER electrocatalytic activity of all the synthesized CDs in an alkaline solution (1 M KOH). The onset potential was generated by drawing tangents in the non-faradaic zone and faradaic zone in LSV curve and the same has been tabulated in Table 2. From the LSV curve (Fig. 8), it is evident that Pt/C catalyst shows the expected HER activity close to zero overpotential. Comparing the synthesized electrocatalysts, the values of overpotential of the synthesized electrocatalysts at − 5 mA cm^{-2} have been tabulated in Table 2. It is observed that S-CDs have the best overpotential value at 1 mV followed by Pt/C at − 29 mV and B-CDs at − 154 mV, respectively. The performance of the synthesized S-CDs electrocatalyst surpassed the performance of Pt/C and hence confirmed that metal-free CDs can outperform traditional catalysts for HER. The enhancement in performance of CDs with incorporation of sulfur can be ascribed to the change in electronic structure, leading to increase in active sites and improvement of charge transfer properties [15, 16]. The overpotential of EDA-CDs was

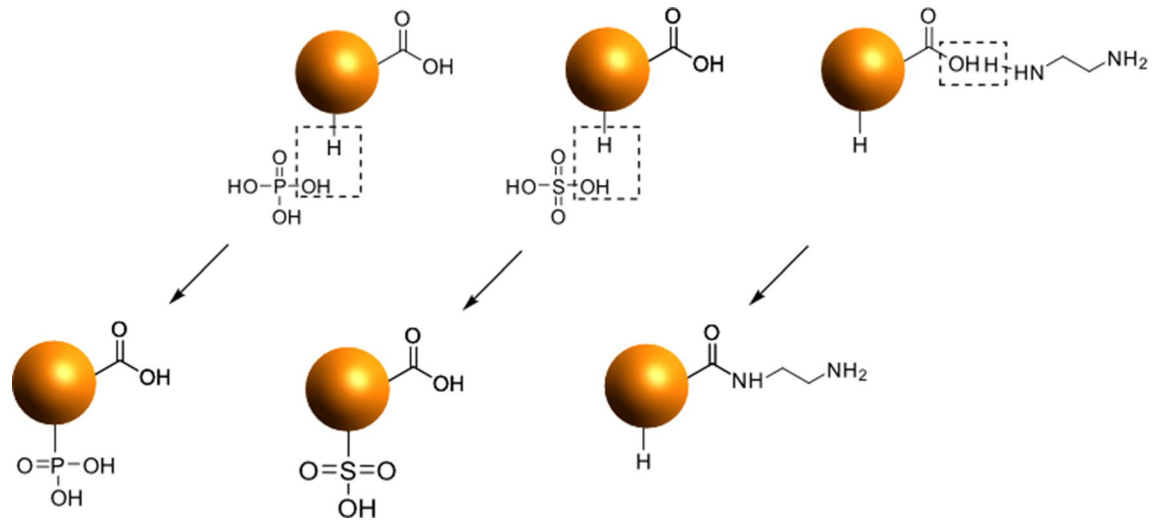

Fig. 7 Possible mechanism involved in the synthesis of CDs

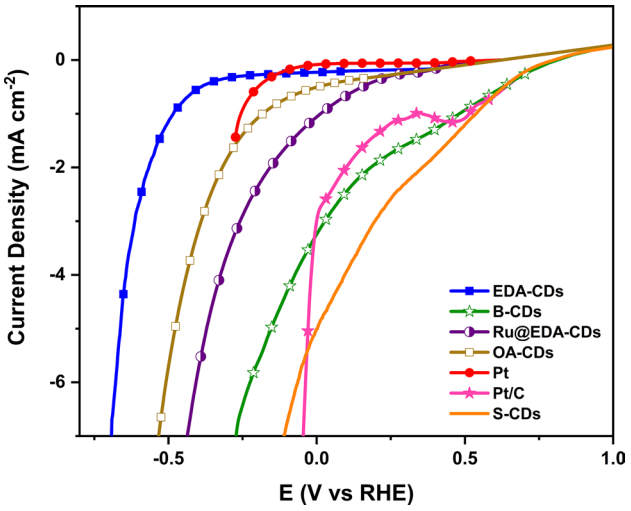

Fig. 8 Polarization curves of CDs at a scan rate of 5 mV s^{-1} in 1M KOH solution

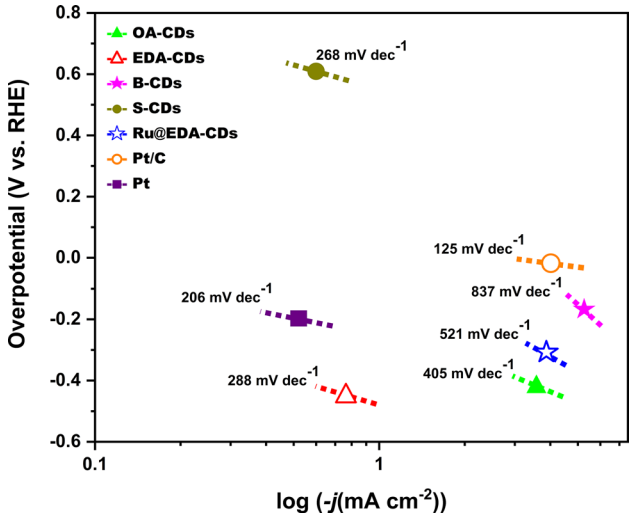

Fig. 10 Tafel plots derived from the corresponding polarization curves of CDs

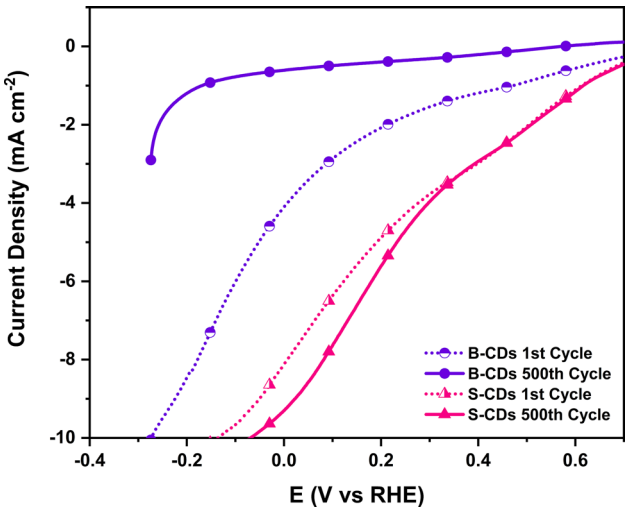

Fig. 9 Polarization curves of CDs at a scan rate of 5 mV s^{-1} in 1M KOH solution after 1st and 500th cycle

Table 2 Onset potential and overpotential of CDs

Sample	Onset potential (mV)	Overpotential (mV)
EDA-CDs	− 451	− 662
OA-CDs	− 253	− 478
Pt	− 198	–
Ru@EDA-CDs	− 48	− 371
Pt/C	10	− 29
B-CDs	61	− 154
S-CDs	237	1

comparatively poor; hence the sample was then subjected to additional capping with Ru to investigate the aided effect of metal. It could be seen that capping of precious metals can significantly improve conductivity of the carrier, modulate the electron distribution to induce a synergistically enhanced reactivity and help tune HER kinetics of CDs based electrocatalysts [17]. Nevertheless, experimental data reported over the years has not been able to clearly conclude if the low HER overpotential is caused by high intrinsic catalytic activities or by extrinsic factors such as increased surface area or mass loading [18]. Figure S1 shows the CV curves of the synthesized CDs recorded at a scan rate of 50 mV s^{-1}.

An important parameter affecting catalytic performance is durability. Figure 9 shows the LSV curves of S-CDs and B-CDs after 500 cycles of CV measurement. It could be observed that S-CDs show exceptional durability with a constant LSV curve. In case of B-CDs, however, the onset potential was found to deteriorate after the 500th cycle. In addition, the current density increases with increasing cycles indicating that the coated CDs catalyst on the surface of electrode apparently corrodes with continuous use. The aforementioned relation between current density and presence of CDs can also be correlated from Fig. 12a and has been verified and discussed in detail in "Effect of CDs in KOH electrolyte".

The Tafel slope is an inherent property of electrocatalyst which is determined from the speed-controlling step of HER. The corresponding Tafel curves of synthesized electrocatalysts are shown in Fig. 10. Pt/C has the lowest Tafel slope at 125 mV dec^{-1}. It is believed that a Tafel slope of 120 mV dec^{-1} arises when the Volmer step becomes the rate-determining step. In the Volmer–Tafel mechanism, the discharge of protons occurs first and on the surface

of catalyst the hydrogen coverage increases [19]. Since graphite was used as catalyst support in our case; it also becomes active towards HER by introducing foreign atoms. Graphite is reported to exhibit Tafel slopes of 208 mV dec^{-1} in 0.1 M KOH. Manuscripts have defined that even theoretical Tafel slopes at small overpotentials do not reach in every case the expected values of 30, 40 and 120 mV dec^{-1} [20]. Amongst the synthesized CDs catalysts, the lowest Tafel slope was observed for S-CDs at 268 mV dec^{-1} followed by EDA-CDs at 288 mV dec^{-1} and OA-CDs at 405 mV dec^{-1}. The performance of S-CDs can be associated with synergistic electronic interactions between the different doped heteroatoms and surrounding carbon atoms resulting in a low Tafel slope [21]. Correspondingly, the Tafel slope of EDA-CDs can be ascribed to nitrogen functionalization, ensuing in reduced charge recombination, optimized charge distribution and structural defects thereby resulting in rapid transfer of ions and electrons [22]. Despite the improved overpotential observed with capping of metals, the Tafel slope was found to degrade in the case of Ru@EDA-CDs as a slope of 521 mV dec^{-1} was seen. Some of the reported Tafel slope results on electrocatalytic materials reported for HER have been enlisted in Table 3. The values of Tafel slope for the synthesized electrocatalysts in 1M KOH are comparatively on the higher end than that reported in previous studies. It is however important to note that high Tafel slopes observed for certain systems (as in our case) are difficult to be explained with simple Volmer–Tafel–Heyrovsky steps which are assumed to describe HER [23]. Since the overpotential values are commendable, a strong basis for the improvement of Tafel slopes of the reported systems can be a priority focus for related research in the domain.

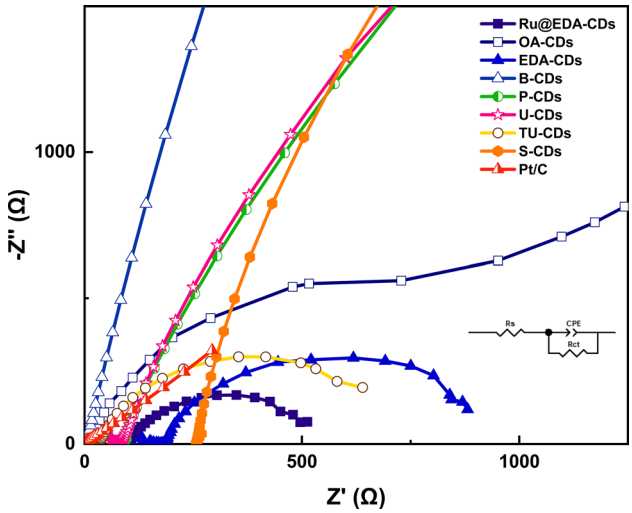

Fig. 11 Nyquist plots of electrochemical impedance spectra of CDs in 1M KOH solution

The electrode dynamics of HER were investigated using the electrochemical impedance spectra. Figure 11 shows the Nyquist curves of the synthesized catalysts. The series (Rs) and charge transfer resistance (Rct) values have been shown in Table 4. Ru@EDA-CDs had the lowest charge transfer resistance, followed by EDA-CDs and Pt/C. In line with previously reported results, Ru@EDA-CDs

Table 3 Comparison of electrocatalysts reported for HER

Catalyst	Carbon precursor	Metal precursor	Electrolyte	Tafel plots (mV dec^{-1})	Overpotential[a] (mV)	Reference
S-CDs	Oleic acid	–	1 M KOH	268	1[#]	This work
EDA-CDs	Oleic acid	–	1 M KOH	288	– 662[#]	This work
OA-CDs	Oleic acid	–	1 M KOH	405	– 478[#]	This work
B-CDs	Oleic acid	–	1 M KOH	837	– 154[#]	This work
Ru@EDA-CDs	Oleic acid	$RuCl_3.3H_2O$	1 M KOH	521	– 371[#]	This work
NiMo film	–	NiMo	1 M KOH	140	– 83[#]	[18]
RuP_2/CDs	Citric acid, l-tryptophan	$RuCl_3.3H_2O$	1 M KOH	63.29	26*	[24]
Ru/CQDs	Ginkgo leaves	$RuCl_3.3H_2O$	1 M KOH	47	0*	[2]
Ru@SC-CDs	Garlic	$RuCl_3.xH_2O$	1 M KOH	57	29*	[25]
G-EX-ST	Graphite powder	-	1 M KOH	80	194*	[26]
Ru@CQDs600	Porphyra	$RuCl_3.xH_2O$	1 M KOH	198	346*	[27]
Ru-Re_3P_4/NPC	MP, NH_4ReO_4	$RuCl_3$	1 M KOH	29	39*	[28]
Pd-CN_x	Formamide	$PdCl_2$	0.5 M KOH	150	– 180[#]	[29]
n-Pd@NDCDs	*Morinda citrifolia*	$PdCl_2$	0.5 M H_2SO_4	135	– 291*	[19]

[a]Sign convention as in reference

[#]At current density of 5 mA cm^{-2}

*At current density of 10 mA cm^{-2}

Table 4 Rs and Rct values corresponding to the equivalent circuit fitting of Nyquist plot

Sample	R_s (Ω cm^2)	Rct (Ω cm^2)
OA-CDs	8.743	1896
EDA-CDs	175.8	780.2
B-CDs	5.422	53530
S-CDs	257.2	15397
Ru@EDA-CDs	102.5	444.1
Pt/C	7.885	1279

exhibit faster interfacial electronic transfer kinetics and higher charge transfer capacity than Pt/C due to the synergic effect between the Ru NPs core and the CDs [2]. The effect reduces the charge-transfer resistance at the catalyst/electrolyte interface, resulting in improved electrochemical conductivity. The overall high charge-transfer impedance can be ascribed to the use of graphite electrode in the process since a high impedance was observed for all the synthesized catalysts including Ru@EDA-CDs.

It is well established that in alkaline systems, HER pathway involves the Volmer–Heyrovsky or Volmer–Tafel steps, with the hydrogen intermediate (H*) following the Volmer step being formed by an initial water dissociation step ($H_2O + e^- \rightarrow H^* + OH^-$). This dissociation produces hydrogen intermediates which get adsorbed in active sites and recombine to yield molecular hydrogen. This step adds an additional energy barrier and is significant in governing HER. Other barriers to HER include deprived water binding energy compared to hydronium ion and poisoning of active sites by OH^- resulting in higher overpotentials. The lower the affinity to OH^- ions the better is the electrocatalyst for alkaline HER. The thermodynamic states of intermediates, kinetic barriers, as well as structural morphology of catalysts significantly affect the HER kinetics. In short, the mechanism behind HER in alkaline electrolyte is complex and still not fully understood [30–32]. With several parameters affecting the performance of electrocatalysts it becomes important to employ modern techniques to fully comprehend the reasoning. Here in our study, it could be seen how subtle changes and addition of new functional groups can significantly alter the HER kinetics. However, the improvement of one parameter did not necessarily equate to improvement in all variables affecting the reaction. This inference implies that the factors affecting HER are complex and more in-depth studies need to be taken up to find the balance of variables for the perfect HER performance.

3.2.2 Effect of CDs in KOH electrolyte

In order to study the influence of CDs solution in electrolyte, Pt electrode was analyzed for HER in 40 mL of 1M KOH. Subsequently, OA-CDs solution viz. 5, 10, 20, 30, 40 mL was added into the electrolyte chamber and the corresponding solutions are named as "Pt-OA-CDs-XmL", respectively, where "*X*" denotes the quantity of CDs. It can be observed from the LSV curve that the onset potential improves by adding CDs in the electrolyte. Moreover, the current density decreases with the addition of CDs i.e., greater the amount of CDs solution added lesser the current density would be. For 30 and 40 mL CDs solution the current density was alike marking the result that the current density decrease trend fails at ratio's higher than (1:0.75)

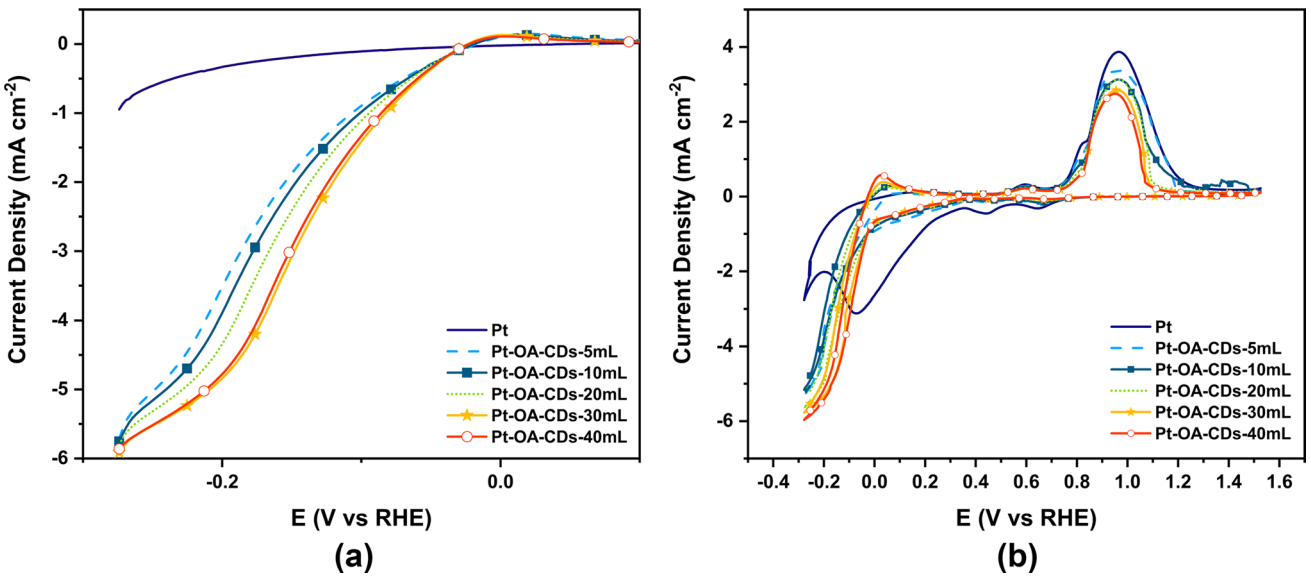

Fig. 12 **a** LSV and **b** CV curve corresponding to the influence of CDs addition in 1M KOH electrolyte

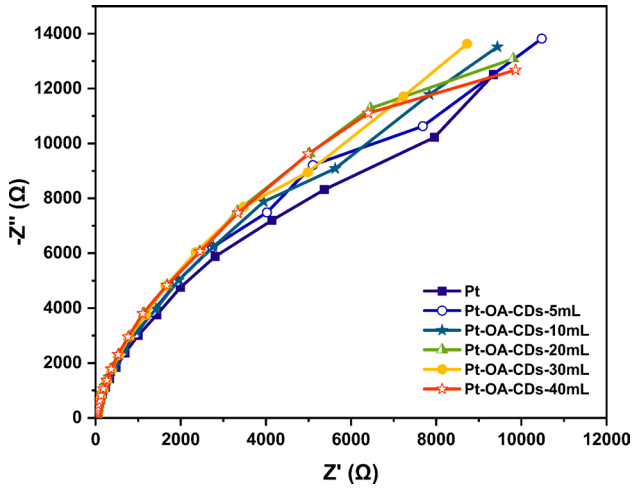

Fig. 13 Nyquist plots of electrochemical impedance spectra corresponding to the influence of CDs addition in 1M KOH electrolyte

between the electrolyte and added CDs. The CV profiles of the electrolyte systems have been displayed in Fig. 12b. 1M KOH had the largest CV loop area with prominent decrease in area being observed with the addition of CDs in the electrolyte. The hydrogen adsorption band characteristic of Pt, was found to be eliminated for "Pt-OA-CDs-XmL" systems but the hydrogen desorption peak non-existent in bare Pt was found to occur and be more pronounced with increasing levels of CDs. The double layer region was consistent in all the systems; however, the oxide formation decreases with addition of CDs. From the Nyquist curves (Fig. 13) it could also be seen that Pt did not illustrate semicircles at the low-frequency region but showed nearly vertical lines for all electrolyte systems, which indicates its low series resistance and high ionic conductivity [3333].

4 Conclusion

In summary, we synthesized oleic acid CDs and investigated the electrocatalytic activity for HER in 1 M KOH. The exceptional activity of functionalized CDs and most importantly low production cost makes them an excellent replacement to Pt/C catalyst. The result promotes the idea that metal-free CDs show high activity for HER in alkaline conditions. It is essential to mention that CDs precursor has a substantial effect on catalytic activity, considering that alike reports using other precursors have not been reported to demonstrate similar electrocatalytic performance without metals. The influence of loading, molecular weight of precursor and functionalizing species viz. N, B, P, S groups have a notable effect on the catalytic activity of oleic acid CDs. In brief, we can say that metal-free CDs show promising results as electrocatalysts for HER and shall serve as ideal replacements to metal counterparts in the near future.

Supplementary Information The online version contains supplementary material available at https://doi.org/10.1007/s10800-022-01780-0.

Acknowledgements Special acknowledgement to the Central Instrumentation Facility, BIT Mesra for the experimental facilities.

References

1. Jain IP (2009) Hydrogen the fuel for 21st century. Int J Hydrog Energy 34(17):7368–7378
2. Li W, Liu Y, Wu M, Feng X, Redfern SA, Shang Y, Yong X, Feng T, Wu K, Liu Z et al (2018) Carbon-quantum-dots-loaded ruthenium nanoparticles as an efficient electrocatalyst for hydrogen production in alkaline media. Adv Mater 30(31):1800676
3. Tian L, Li Z, Wang P, Zhai X, Wang X, Li T (2021) Carbon quantum dots for advanced electrocatalysis. J Energy Chem 55:279–294
4. Wang J, Kong H, Zhang J, Hao Y, Shao Z, Ciucci F (2021) Carbon-based electrocatalysts for sustainable energy applications. Prog Mater Sci 116:100717
5. Rimal V, Shishodia S, Srivastava PK, Gupta S, Mallick AI (2021) Synthesis and characterization of Indian essential oil carbon dots for interdisciplinary applications. Appl Nanosci 11(4):1225–1239
6. Yao B, Huang H, Liu Y, Kang Z (2019) Carbon dots: a small conundrum. Trends Chem 1(2):235–246
7. Huang D, Chen Y, Cheng M, Lei L, Chen S, Wang W, Liu X (2021) Carbon dots-decorated carbon-based metal-free catalysts for electrochemical energy storage. Small 17(4):2002998
8. Liu Y, Roy S, Sarkar S, Jiaqiang X, Zhao Y, Zhang J (2021) A review of carbon dots and their composite materials for electrochemical energy technologies. Carbon Energy 3(5):795–826
9. Rimal V, Shishodia S, Srivastava PK (2020) Novel synthesis of high-thermal stability carbon dots and nanocomposites from oleic acid as an organic substrate. Appl Nanosci 10(2):455–464
10. Khan WU, Wang D, Zhang W, Tang Z, Ma X, Ding X, Du S, Wang Y (2017) High quantum yield green-emitting carbon dots for Fe (iii) detection, biocompatible fluorescent ink and cellular imaging. Sci Rep 7(1):1–9
11. González-González RB, González LT, Madou M, Leyva-Porras C, Martinez-Chapa SO, Mendoza A (2022) Synthesis, purification, and characterization of carbon dots from non-activated and activated pyrolytic carbon black. Nanomaterials 12(3):298
12. Jastrzebski W, Sitarz M, Rokita M, Bułat K (2011) Infrared spectroscopy of different phosphates structures. Spectrochim Acta Part A 79(4):722–727
13. Vinayan BP, Zhao-Karger Z, Diemant T, Chakravadhanula VSK, Schwarzburger NI, Cambaz MA, Behm RJ, Kübel C, Fichtner M (2016) Performance study of magnesium-sulfur battery using a graphene based sulfur composite cathode electrode and a non-nucleophilic mg electrolyte. Nanoscale 8(6):3296–3306
14. Yan F, Jiang Y, Sun X, Bai Z, Zhang Y, Zhou X (2018) Surface modification and chemical functionalization of carbon dots: a review. Microchim Acta 185(9):1–34
15. Mabayoje O, Wygant BR, Wang M, Liu Y, Mullins CB (2018) Sulfur-rich mos6 as an electrocatalyst for the hydrogen evolution reaction. ACS Appl Energy Mater 1(9):4453–4458

16. Cheng R, Jiang M, Li K, Guo M, Zhang J, Ren J, Meng P, Li R, Chaopeng F (2021) Dimensional engineering of carbon dots derived sulfur and nitrogen co-doped carbon as efficient oxygen reduction reaction electrocatalysts for aluminum-air batteries. Chem Eng J 425:130603
17. Yang Y, Yanhui Yu, Li J, Chen Q, Yanlian D, Rao P, Li R, Jia C, Kang Z, Deng P et al (2021) Engineering ruthenium-based electrocatalysts for effective hydrogen evolution reaction. Nano-Micro Lett 13(1):1–20
18. Bao F, Kemppainen E, Dorbandt I, Bors R, Xi F, Schlatmann R, van de Krol R, Calnan S (2021) Understanding the hydrogen evolution reaction kinetics of electrodeposited nickel-molybdenum in acidic, near-neutral, and alkaline conditions. ChemElectroChem 8(1):195–208
19. Chandrasekaran P, Edison TN, Sethuraman MG (2020) Electrocatalytic performance of carbon dots/palladium nanoparticles composite towards hydrogen evolution reaction in acid medium. Int J Hydrog Energy 45(53):28800–28811
20. Shinagawa T, Garcia-Esparza AT, Takanabe K (2015) Insight on Tafel slopes from a microkinetic analysis of aqueous electrocatalysis for energy conversion. Sci Rep 5(1):1–21
21. Liu X, Dai L (2016) Carbon-based metal-free catalysts. Nat Rev Mater 1(11):1–12
22. Feng T, Tao S, Yue D, Zeng Q, Chen W, Yang B (2020) Recent advances in energy conversion applications of carbon dots: from optoelectronic devices to electrocatalysis. Small 16(31):2001295
23. Morozan A, Goellner V, Nedellec Y, Hannauer J, Jaouen F (2015) Effect of the transition metal on metal-nitrogen-carbon catalysts for the hydrogen evolution reaction. J Electrochem Soc 162(9):H719
24. Song H, Cheng Y, Li B, Fan Y, Liu B, Tang Z, Siyu L (2020) Carbon dots and rup2 nanohybrid as an efficient bifunctional catalyst for electrochemical hydrogen evolution reaction and hydrolysis of ammonia borane. ACS Sustain Chem Eng 8(9):3995–4002
25. Liu Y, Yang Y, Peng Z, Liu Z, Zhimin Chen L, Shang SL, Zhang T (2019) Self-crosslinking carbon dots loaded ruthenium dots as an efficient and super-stable hydrogen production electrocatalyst at all ph values. Nano Energy 65:104023
26. Zhao M, Zhang J, Xiao H, Tianjun H, Jia J, Haishun W (2019) Facile in situ synthesis of a carbon quantum dot/graphene heterostructure as an efficient metal-free electrocatalyst for overall water splitting. Chem Commun 55(11):1635–1638
27. Li W, Wei Z, Wang B, Liu Y, Song H, Tang Z, Yang B, Siyu L (2020) Carbon quantum dots enhanced the activity for the hydrogen evolution reaction in ruthenium-based electrocatalysts. Mater Chem Front 4(1):277–284
28. Gao Y, Zhao Y, Liu H, Shao M, Chen Z, Ma T, Zexing W, Wang L (2022) N, p-doped carbon supported ruthenium doped rhenium phosphide with porous nanostructure for hydrogen evolution reaction using sustainable energies. J Colloid Interface Sci 606:1874–1881
29. Bhowmik T, Kundu MK, Barman S (2016) Palladium nanoparticle-graphitic carbon nitride porous synergistic catalyst for hydrogen evolution/oxidation reactions over a broad range of ph and correlation of its catalytic activity with measured hydrogen binding energy. ACS Catal 6(3):1929–1941
30. Mahmood N, Yao Y, Zhang J-W, Pan L, Zhang X, Zou J-J (2018) Electrocatalysts for hydrogen evolution in alkaline electrolytes: mechanisms, challenges, and prospective solutions. Adv Sci 5(2):1700464
31. Zheng Y, Jiao Y, Vasileff A, Qiao S-Z (2018) The hydrogen evolution reaction in alkaline solution: from theory, single crystal models, to practical electrocatalysts. Angew Chem Int Ed 57(26):7568–7579
32. Bie C, Wang L, Yu J (2022) Challenges for photocatalytic overall water splitting. Chemistry
33. Pholauyphon W, Bulakhe RN, Manyam J, In I, Paoprasert P (2022) High-performance supercapacitors using carbon dots/titanium dioxide composite electrodes and carbon dot-added sulfuric acid electrolyte. J Electroanal Chem 910:116177